Effects of cytosine methylation on DNA morphology: an atomic force microscopy study

V. Cassina[a], M. Manghi[b], D. Salerno[a], A. Tempestini[c], V. Iadarola[a], L. Nardo[a], S. Brioschi[a], F. Mantegazza[a]

[a]*Health Science Department, University of Milano-Bicocca, Via Cadore 48, 20900, Monza (MB), Italy*
[b]*Laboratoire de Physique Théorique, Université Paul Sabatier, CNRS, 118 route de Narbonne, 31062 Toulouse, France*
[c]*LENS-Dipartimento di Fisica e Astronomia, Universitá degli studi di Firenze, via Sansone 1, 50019, Sesto Fiorentino (FI), Italy*

Abstract

Methylation is one of the most important epigenetic mechanisms in eukaryotes. As a consequence of cytosine methylation, the binding of proteins that are implicated in transcription to gene promoters is severely hindered, which results in gene regulation and, eventually, gene silencing. To date, the mechanisms by which methylation biases the binding affinities of proteins to DNA are not fully understood; however, it has been proposed that changes in double-strand conformations, such as stretching, bending, and over-twisting, as well as local variations in DNA stiffness/flexibility may play a role. The present work investigates, at the single molecule level, the morphological consequences of DNA methylation in vitro. By tracking the atomic force microscopy images of single DNA molecules, we characterize DNA conformations pertaining to two different degrees of methylation. In particular, we observe that methylation induces no relevant variations in DNA contour lengths, but produces measurable incremental changes in persistence lengths. Furthermore, we observe that for the methylated chains, the statistical distribution of angles along the DNA coordinate length is characterized by a double exponential decay, in agreement with what is predicted for polyelectrolytes. The results reported herein support the claim that the biological consequences of the methylation process, specifically difficulties in protein-DNA binding, are at least partially due to DNA conformation modifications.

Keywords: DNA Methylation, Atomic force Microscopy (AFM), Persistence length

1. Introduction

Cytosine methylation naturally occurs in the genomes of different organisms and represents a well-known epigenetic mechanism for regulating gene expression. DNA methylation is not homogeneously distributed throughout each genome but appears to be concentrated in specific hotspots that are enriched in cytosine-guanine dinucleotides called CpG islands. Over the last 20 years, our comprehension of DNA methylation has notably improved, and it is now understood that this methylation mechanism is involved in X-chromosome inactivation [1], genomic imprinting [2], cell development and differentiation [3], and biological aging [4]. Furthermore, in humans, aberrant methylation results in the emergence of severe diseases [5, 6]. When methylation at CpG sites occurs within gene promoters or enhancers or adjacent to transcription start sites, it induces the robust transcriptional repression of downstream genes. This effect is primarily achieved by inhibiting the binding of transcription factors to the above-mentioned DNA traits. Consequently, the recruitment of RNA-polymerase complexes is hindered. Nevertheless, the mechanisms by which CpG methylation induces such dramatic reductions in transcription factors affinities for their DNA binding sites and, therefore, the mechanisms by which gene silencing occurs remain controversial [7, 8, 9]. Another topic of interest is whether DNA methylation confers different morphological properties to the DNA double-strand. The above issues are perhaps related, inasmuch as transcriptional repression might be a consequence of DNA conformation alterations caused by cytosine methylation. The notorious increase in the thermodynamic stability of the double-stranded structure of methylated versus non-methylated DNA [10, 11, 12] supports the hypothesis that DNA flexibility is affected accordingly.

To date, few single-molecule investigations of DNA

*Correspondence to: Valeria Cassina, Health Science Department, University of Milano-Bicocca, Via Cadore 48, 20900, Monza (MB) Italy

Email address: valeria.cassina@unimib.it (V. Cassina)

methylation have been presented in literature, and the few reports primarily utilize atomic force microscopy (AFM) [13]. AFM is a powerful and widespread tool in biophysical research and is used both to image biological samples with nanometer resolution [14, 15] and to investigate single molecule nanomechanics by means of force spectroscopy method [16, 17]. Such AFM studies enable researchers to make relevant conclusions regarding methylated DNA morphology. Both DNA short segments [18] and DNA-chromatin complexes [19, 20] have been studied using AFM, thus demonstrating the ability of this technique to detect statistical variations in DNA flexibility and to be utilized in different situations. AFM studies have also revealed that the compaction of chromatin that has been reconstituted on methylated DNA depends on hydration levels [21]. When used in force spectroscopy mode, AFM has also revealed DNA methylation patterns by measuring the distances between methylated bases [22]. Furthermore, AFM has been used to shear and to unzip methylated DNA oligonucleotides to investigate the effects of methylation on strand separation, thereby revealing a dependence on the degrees of methylation and the localization of methylated sites along the chain [23]. A completely different approach, which exploits DNA origami scaffolds and utilizes AFM imaging, has been used to apply different double-helical tensions to methylated DNA samples and control the methyl transfer reaction of M.EcoRI [24].

The present study utilizes AFM to obtain nanometer-resolution images of DNA molecules that have been deposited on atomically flat surfaces [25, 26, 27], with the aim of characterizing the DNA conformations that result from different levels of methylation. In addition to qualitatively analyzing the resulting AFM images, the methylation effects are quantitatively characterized using the parameters of contour length (L_c) and persistence length (L_p) to describe each specific DNA conformation [14, 28, 29, 30]. We note that the contour length L_c of a DNA chain is the length at its maximum extension and that the persistence length L_p is the basic mechanical property that quantifies DNA chain stiffness, which corresponds to the average distance along which the DNA maintains its direction before deviating from it. The results reported herein indicate that the methylation process induces a measurable increase in persistence length and no relevant variation in contour length. These results support the notion that differences in DNA conformation may contribute to the biological effects connected to DNA methylation [23].

2. Materials and methods

DNA preparation and methylation. The pCMV6-Neo plasmid was linearized with NotI and SacII restriction enzymes, which led to a 5780 bp-long DNA molecule (hereafter called bare). All of the enzymes used in this work were obtained from New England Biolabs (NEB). To obtain different methylation levels we used different enzymes in condition of fully saturating reaction, i.e. reaction time, and SAM and enzymes concentrations overwhelmingly exceeded those reported in the datasheets. In the first reaction, which targeted CpG traits, 1 μg of the linearized plasmid DNA template was added to s-adenosine methionine (SAM, 2 μl 160 μM) followed by the addition of ten units of CpG Methyltransferase (M.SssI) and 2 μl NEB buffer 2 (New England Biolabs). The mixture was diluted to 20 μl final volume and incubated at 37°C for 5 h. Since SAM is unstable at 37°C, and should be replenished for reactions incubated longer than 4 hours, 1 μl 160 μM SAM was added to the reaction volume every hour (800 μM final concentration). This procedure resulted in full methylation of the CpG dinucleotides, as indicated by the gel results (Fig.1(a)) (on average, 1 base on 16, 5.8% of the total base pairs, or 22% of the cytosines, mild methylation [23], hereafter called Met1). The second methylation reaction (which targeted GpC dinucleotides) uses the DNA Met1 as the initial DNA substrate. As in the first methylation reaction, 1 μg of the DNA template (Met1) was added to s-adenosine methionine (SAM, 2 μl 160 μM) followed by the addition of ten units of GpC Methyltransferase (M.CviPI) (New England Biolabs) and 2 μl NEB buffer 2 (New England Biolabs). The mixture was diluted to 20 μl final volume and incubated at 37°C for 5 h. Since SAM is unstable at 37°C, and should be replenished for reactions incubated longer than 4 hours, 1 μl 160 μM SAM was added to the reaction volume every hour (800 μM final concentration). This procedure resulted in full methylation of GpC dinucleotides, as indicated by the gel results (Fig.1(b)) (on average, 1 base on 8, 11.8% of the total base pairs, or 46% of the cytosines, strong methylation, hereafter called Met2).

The efficiency of the methylation process was confirmed by digesting the DNA Met1 and DNA Met2 samples with enzymes for which cleavage is blocked when the recognition sequences are methylated (BstBI or HaeIII, respectively). The agarose gels of the digested products of BstBI or HaeIII enzymes and both bare DNA and Met1 or Met2 DNA are shown in Fig.1. These enzymes cut the bare DNA (lane 4) and were inactive with regard to the methylated DNA (lane 3). The

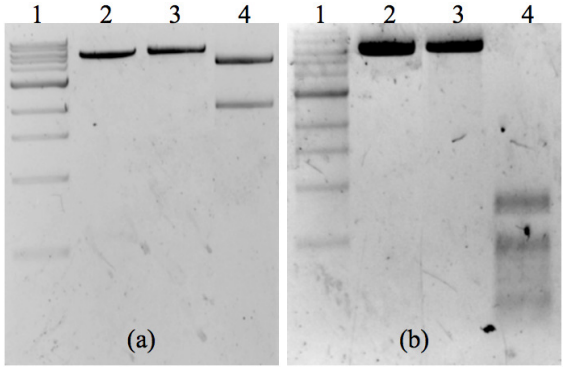

Figure 1: (a) BstBI digestion products of methylated DNA Met1 and control DNA analyzed on a 1.2% agarose gel. Lane 1: 1 kb ladder (NEB); Lane 2: bare DNA (linearized pCMV6-Neo), not treated with M.SssI or BstBI; Lane 3: Met1 DNA, previously treated with M.SssI and incubated with BstBI; Lane 4: bare DNA, not treated with M.SssI and incubated with BstBI. (b) HaeIII digestion products of methylated DNA Met2 and control DNA analyzed on a 1.2% agarose gel. Lane 1: 1 kb ladder (NEB); Lane 2: bare DNA (linearized pCMV6-Neo), not treated with M.CviPI or HaeIII; Lane 3: Met2 DNA, previously treated with M.CviPI and incubated with HaeIII; Lane 3: bare DNA, not treated with M.CviPI and incubated with HaeIII.

presence of unmethylated sites would results in the presence of low molecular weight bands in the gel, which actually are not detectable. Visualization of 10 ng of DNA is typically possible in an agarose gel stained with ethidium bromide. In Fig.1(a) 200 ng of DNA were loaded in each line and, since no digestion bands are visible in line 3, then the Met1 DNA should have at least 95% of methylated CpG dinucleotides. In Fig.1(b) 500 ng of DNA were loaded in each line; since the stronger band in line 4 corresponds approximately to 150 ng and since no digestion bands are visible in line 3, then the Met2 DNA should have at least 93% of methylated GpC dinucleotides. Thus, DNA strands that were protected from digestion were confirmed to be methylated and were subsequently used for AFM experiments.

Sample preparation. Each of the three different DNA preparations was diluted to a final concentration of ~0.2 ng/μl in 5 mM $MgCl_2$ buffer. The DNA concentration used in these studies was estimated such that reasonable DNA molecule statistics could be expected and single filament deposition could be achieved on mica without chain superposition. To study the modifications of DNA morphology upon methylation, 35 μl of the DNA solution was incubated on freshly cleaved mica (Ted Pella) at room temperature for 5 min to allow the DNA to adsorb to the surface. The sample was rinsed with 0.22 μm-filtered de-ionized pure water and dried with a gentle nitrogen flow.

AFM imaging. AFM images of DNA were acquired using a Nanowizard II (JPK Instruments, Berlin) instrument. Measurements were performed in tapping mode in air, and 4μm x 4μm images were acquired using a 1-Hz scan rate with 1024 x 1024-pixel resolution. All data in this study were verified by sampling a wide range of areas over the sample surfaces and analyzing hundreds of filaments for each of the three samples.

Image analysis. To determine the characteristic morphological quantities of the samples, i.e. contour lengths (L_c) and persistence lengths (L_p), we developed a customized image-analysis software program to automatically track (with human supervision) the DNA molecules. The procedure is analogous to others validated algorithms [31]. A representative AFM image of bare DNA is shown in Fig.2a. The output of the algorithm procedure provides the coordinates of the geometric 2D shape of every single filament (red dots in Fig.2). The tracking algorithm is sketched in Fig.2b and Fig.2c. Basically, the procedure recognizes the DNA trace in the x-y plane as an ensemble of points of higher altitude with respect to the average height of the mica. The algorithm proceeds as follows: (i) First, the operator manually places an initial point on one end of the filament under examination, a tracking direction of the DNA filament, and a final point on the other end. (ii) Then, a trial circumference (radius = 3 pixels ~15 nm), centered in the initial point (blue dot named *current point* in the figure) is traced. (iii) A trial point is placed at the maximum z height along the circumference (excluding the previous point on iteration). (iv) The point corresponding to the higher nearest neighbor to the trial point is defined as the new initial point (white dot in figure). This process is repeated until the end of the filament is reached. (v) The coordinates obtained in this way are used as the predefined points for a spline interpolation that gives back the DNA x-y coordinates schematized as a skeleton of joined segments of 5-nm lengths (red dots in Fig.2).

3. Results and discussion

Fig.3 shows representative AFM images of each sample investigated: bare DNA (Fig.3a), Met1 DNA (Fig.3b), Met2 DNA (Fig.3c). Bare DNA appears as flexible filaments, Met1 DNA molecules have slightly more elongated morphologies, whereas Met2 DNA chains appear to have more stretched configurations. Thus, at least by visual inspection, DNA molecules with higher methylation levels appear to be more elongated. In addition to the qualitative examination of the sample

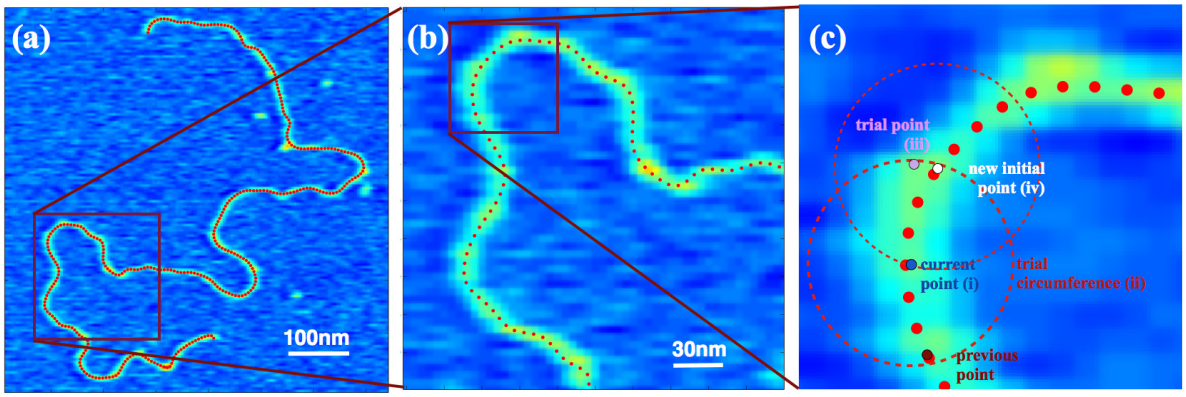

Figure 2: Representative *(a)* and magnified *(b)* AFM images of a DNA molecule tracked using a semi-automated Matlab routine (z-range 1.5 nm). The trace (red dots) was obtained as shown in panel *(c)*.

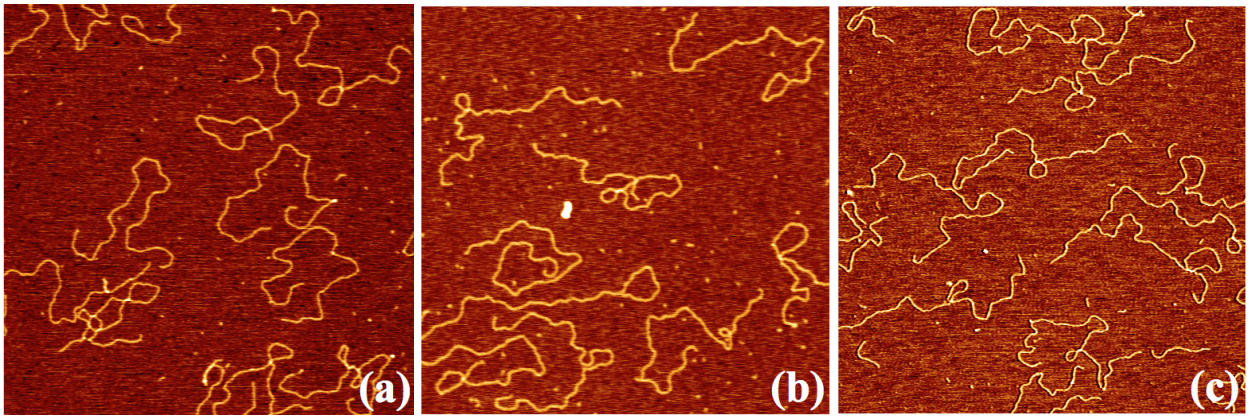

Figure 3: Representative AFM images (2 μm x 2 μm, z-range 1.5 nm) of single DNA filaments on mica. *(a)* Bare DNA; *(b)* Met1 DNA; *(c)* Met2 DNA.

images, AFM allows measuring quantitatively the DNA physical characteristics by giving access to the contour length and the persistence length.

After drawing the trace coordinates for each filament, the contour length L_c is calculated as the total summation of the tracked segment lengths. Fig.4 displays histograms of the contour lengths obtained for both the bare DNA and the two methylated samples. L_c displays a statistical distribution, such that the average contour length $\langle L_c \rangle$ of each experimental set can be determined via a Gaussian fit to the contour-length histogram of every tracked filament. On average, the contour length $\langle L_c \rangle$ is approximately 1810 ± 70 nm and appears not to be significantly influenced by methylation. We note that the average DNA contour length is compatible with the base-pair number (5780 bp) of the DNA sample under study. Furthermore, given the chemical binding of the methylation group, which is located external to the DNA double strand, it is reasonable that we do not observe any relevant variations in DNA extensions due to varying methylation levels. These conclusions are compatible with analogous results that have appeared recently in the literature, for which no definitive conclusions regarding DNA extension as a consequence of methylation could be drawn [21].

The standard procedure used to extract the DNA persistence length from AFM images is based on an analysis of the mean square end-to-end distance $\langle (R_{s,s+L})^2 \rangle$ between a pair of points located along contour length s and $s + L$, measured along the chain and averaged over the curvilinear coordinate s [31, 32]. For each set of experiments, $\langle (R_{s,s+L})^2 \rangle$ is obtained as a function of the separation L by averaging the measurements taken from hundreds of DNA tracked filaments. Accordingly, Fig.5 plots the $\langle (R_{s,s+L})^2 \rangle$ data for both the bare DNA and the two methylated DNA samples. The resulting data were fitted according to the following expression, which is related to the two-dimensional Worm-Like-Chain (WLC)

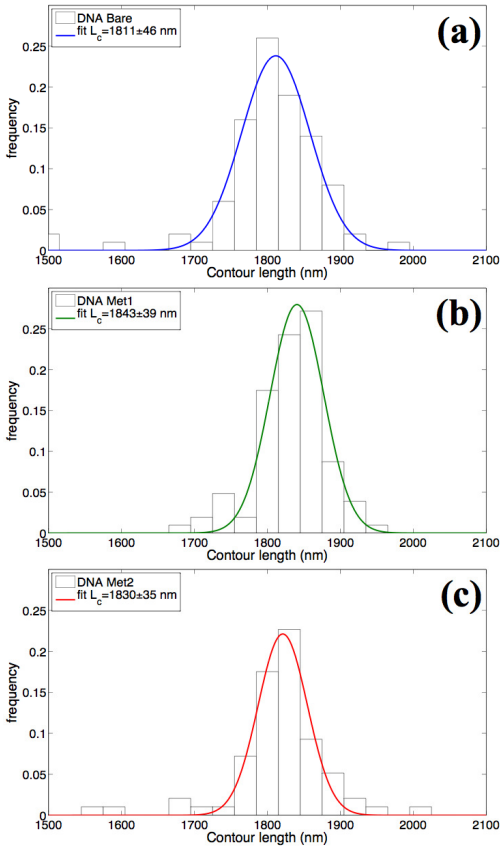

Figure 4: Histograms of contour-length L_c values measured from AFM images and relative Gaussian fits for bare DNA *(a)*, Met1 DNA *(b)*, and Met2 DNA *(c)*.

model, taking the persistence length L_p as the free parameter of the fit [31, 32]:

$$\langle (R_{s,s+L})^2 \rangle = 2(2L_p)^2 \left(\frac{L}{2L_p} - 1 + e^{-\frac{L}{2L_p}} \right) \qquad (1)$$

Note that, in Eq.1, L_p is the three-dimensional persistence length, related to the bending modulus κ by $L_p = a\kappa/k_BT$ (where k_BT is the thermal energy, and a is the base-pair length).

As shown in Fig.6, the fitting model described by Eq.1 describes well the data obtained from all three samples up to separation distance L values of 500 nm. Beyond this value, the data are typically noisy and systematically different from the fitting curve. By means of this procedure, the L_p values are evaluated at different levels of methylation (see Fig.6), thus obtaining $L_p^{R^2} = 56.6 \pm 3.5$ nm (bare DNA), $L_p^{R^2} = 67.2 \pm 4$ nm (Met1 DNA), and $L_p^{R^2} = 70.6 \pm 4.4$ nm (Met2 DNA).

The persistence-length increase due to the presence of methylation is also confirmed by considering the average values of the tangent-tangent correlation function $\langle \cos(\theta_{s,s+L}) \rangle$, where $\theta_{s,s+L}$ is the angle between the tangent vectors of a pair of points separated by a curvilinear distance L. Under equilibrium conditions, the angle (or tangent-tangent) correlation function shows exponential decaying behavior as follows [32]:

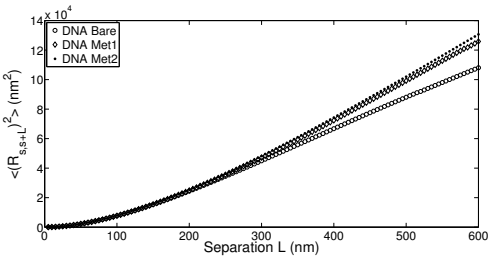

Figure 5: Measured mean square values of the end-to-end distances $\langle (R_{s,s+L})^2 \rangle$ plotted as a function of the separation L along the curvilinear distance s for bare DNA *(circles)*, Met1 DNA *(diamonds)* and Met2 DNA *(dots)*.

$$\langle \cos(\theta_{s,s+L}) \rangle = e^{-\frac{L}{2L_p}} \qquad (2)$$

Accordingly, Fig.7 presents the $\langle \cos(\theta_{s,s+L}) \rangle$ data for bare and methylated DNA, and Fig.8 shows the fits obtained using Eq.2. The L_p values obtained are, respectively, $L_p^{\cos\theta} = 57 \pm 5$ nm (bare DNA), $L_p^{\cos\theta} = 65.7 \pm 8$ nm (Met1 DNA), and $L_p^{\cos\theta} = 68.2 \pm 9.5$ nm (Met2 DNA). These values were obtained irrespective of the quality of the fit, for which the results are less convincing with respect to the fits shown in Fig.6. This procedure also confirms the obtained L_p increase corresponding to the methylation levels. Thus, the value of the L_p parameter, based on fitting the data in Fig.8, shows an increase at high methylation levels in agreement with the results obtained via the end-to-end fitting procedure (Fig.6). Overall, the persistence lengths appear to depend on the corresponding methylation levels (Fig.9), thus demonstrating an increase of DNA rigidity that is dependent on the presence of methylation. These results were confirmed by other authors, who suggested that variations in DNA stiffness constitute the commencement of a possible mechanism of gene silencing as a result of the interaction of methylated DNA with nucleosomes [21, 33].

However, the description of the data pertaining to $\langle \cos(\theta_{s,s+L}) \rangle$ with a single decaying exponential do not appear to completely characterize the physical system under examination. Other authors have suggested that more complex models must be used to describe the behavior of charged polyelectrolyte chains [34, 35, 36]. We adopted this approach to analyze the effects of

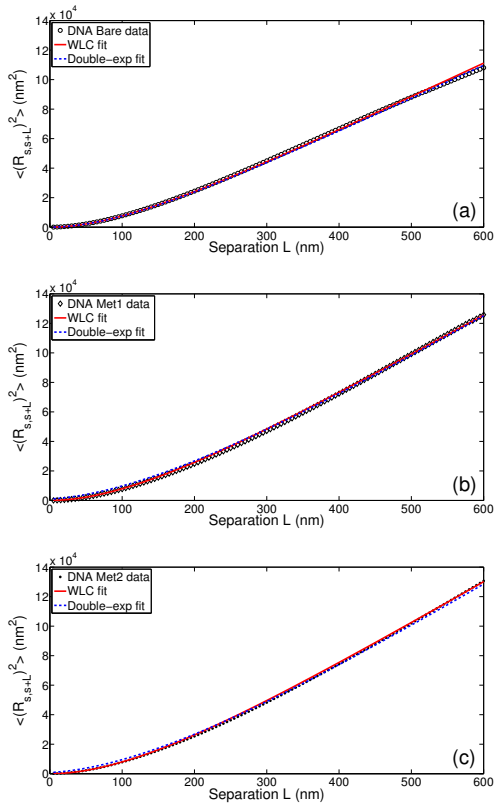

Figure 6: *Symbols*: mean square values of the end-to-end distances $\langle (R_{s,s+L})^2 \rangle$ plotted as a function of the separation L along the curvilinear distance s for bare DNA *(a)*, Met1 DNA *(b)* and Met2 DNA *(c)*. *Red lines*: WLC model fit (Eq.1) with persistence length $L_p^{R^2}$ as the free parameter. *Blue lines*: double exponential fitting model (Eq.3). The fitting parameter values obtained are reported in Tab.1. Both fitting models describe the data well and are almost indistinguishable.

methylation on DNA morphology, as described below. In particular, at small length scales, DNA does not feel the methylation and has a bare intrinsic persistence length L_0. In addition, as suggested by the experiments described herein, the methylated DNA persistence length is larger at large length scales: $L_+ = L_0 + L_e$, where L_e is an additional persistence length. Consequently, it is possible to predict the following expressions pertaining to the end-to-end distance $\langle (R_{s,s+L})^2 \rangle$ and the tangent-tangent correlation function $\langle \cos(\theta_{s,s+L}) \rangle$ [34]:

$$\langle (R_{s,s+L})^2 \rangle = 2B(2L_+)^2 \left(\frac{L}{2L_+} - 1 + e^{-\frac{L}{2L_+}} \right) \qquad (3)$$
$$+2(1-B)(2L_-)^2 \left(\frac{L}{2L_-} - 1 + e^{-\frac{L}{2L_-}} \right)$$
$$\langle \cos(\theta_{s,s+L}) \rangle = Be^{-\frac{L}{2L_+}} + (1-B)e^{-\frac{L}{2L_-}} \qquad (4)$$

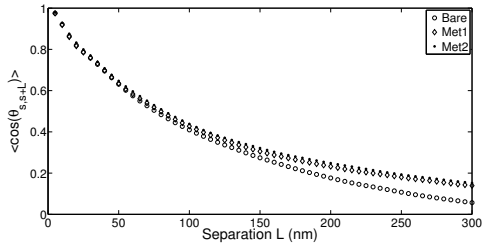

Figure 7: Measured mean square values of the end-to-end distances $\langle \cos(\theta_{s,s+L}) \rangle$ plotted as a function of the separation L along the curvilinear distance s for bare DNA *(circles)*, Met1 DNA *(diamonds)* and Met2 DNA *(dots)*.

DNA	Bare	Met1	Met2
$L_p^{R^2}$	56.6 ± 3.5	67.2 ± 4	70.6 ± 4.4
$L_p^{\cos\theta}$	57 ± 5	65.7 ± 8	68.2± 9.5
L_0	51.3 ± 3.6	50.0 ± 5.1	51.5 ± 4.2
L_e	6.1 ± 3.4	48.5 ± 4.3	47.5 ± 4.9
$L_+ = L_0 + L_e$	57.4	98.45	99
L_-	8.5	28	27.5
B	0.979	0.61	0.643
s_c	20	100	95

Table 1: Fitting parameters obtained with the different methods used herein as a function of methylation fraction. All lengths are in nm. The crossover distances s_c are calculated according to Eq.6.

where

$$L_+ = L_0 + L_e, \qquad L_- = \frac{(1-B)L_0(L_0+L_e)}{L_e + (1-B)L_0} \qquad (5)$$

and $0 \leq B \leq 1$ is the weight of the exponential decrease with persistence length L_+. Eqs.4-3 are a generalization of Eqs.1-2 with a double exponential decrease. In particular, in the limit $L_e = 0$ (no methylation), one has $L_+ = L_- = L_0$, and one recovers the single exponential decrease Eqs.1-2.

Overall, the resulting equations introduce a second exponential decay due to the effects of methylation on flexibility. As reported in Fig.6 and Fig.8, the above models enable a more accurate fitting of the data. For each sample, both the $\langle (R_{s,s+L})^2 \rangle$ and $\langle \cos(\theta_{s,s+L}) \rangle$ were fitted with the same parameters set for each DNA sample. For the $\langle (R_{s,s+L})^2 \rangle$ data, the two equations (Eq.1 and Eq.3) give similar results (see Fig.6). However, for the $\langle \cos(\theta_{s,s+L}) \rangle$ data, better agreement between the two-exponential theory (Eq.3 and Eq.4) and the experimental results is clearly evident (see Fig.8). The resulting fitting parameters (L_e and L_0) are reported in Tab.1 and are shown in Fig.9, together with the classical WLC model parameters (i.e. $L_p^{R^2}$ and $L_p^{\cos\theta}$) obtained as a function of methylation percentage. Overall,

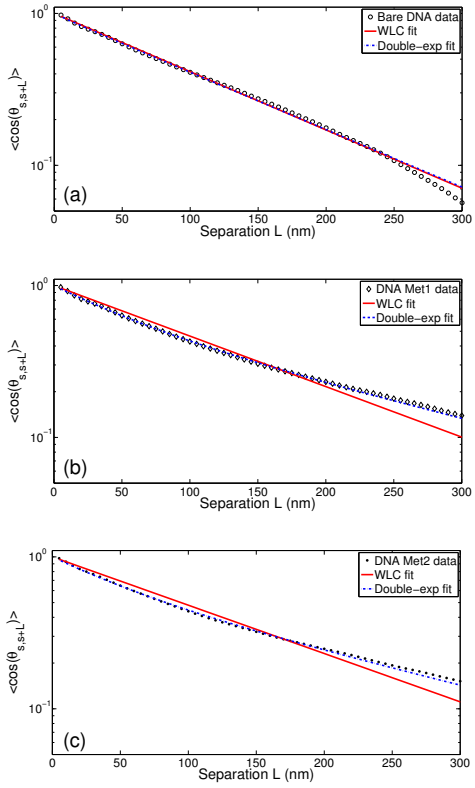

Figure 8: *Symbols*: mean values $\langle\cos(\theta_{s,s+L})\rangle$ plotted as a function of the separation L along the curvilinear distance s for bare DNA *(a)*, Met1 DNA *(b)* and Met2 DNA *(c)*. *Red lines*: WLC fitting model (Eq.2) with persistence length $L_p^{\cos\theta}$ as the free parameter. *Blue lines*: double exponential fitting model (Eq.4). The fitting parameter values obtained are reported in Tab.1.

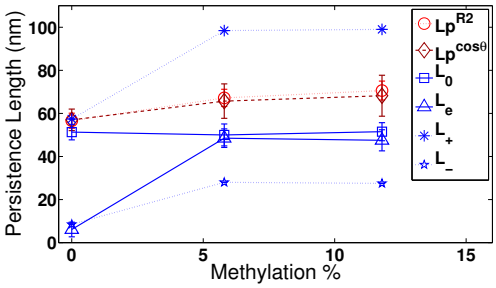

Figure 9: Fitting parameters obtained with both the WLC method *(red symbols and lines)* and the two-exponential method *(blue symbols and lines)* as a function of methylation fraction. The methylation percentage is calculated as the number of CpG and CpG+GpC sites over the total number of base pairs of the DNA filaments.

we note that the increase of L_e depends on the methylation level but that L_0 is basically constant (or slightly decreasing) and equal to the intrinsic three-dimensional DNA persistence length ($\sim$ 50 nm) [32, 37]. In particular, we find that the L_e value for bare DNA is very small, whereas it increases abruptly for Met1 DNA and Met2 DNA. However, it should be noted that a non-simply linear dependence of several physical properties of DNA on the cytosine methylation extent agrees with several literature reports [38, 39, 21, 18, 40].

Thus, the two-exponential model seems to be a reasonable approach and indicates that, at small length scales and on average, the DNA under study does not feel the corresponding methylation and maintains its bare persistence length. At large length scales, however, the DNA chain feels the methylation, which seems to stiffen it.

The crossover curvilinear index s_c between the behavior at short distances in $1 - \frac{L}{2L_0}$ and at longer distances in $B\exp[-L/(2L_+)]$ is given by

$$s_c = -2\frac{L_0(L_0 + L_e)}{L_e}\ln(B) \qquad (6)$$

The values of this crossover index are given in Table1 and correspond to the changes in the slopes in Fig.8.

The two-exponential model has been developed to describe increases in the persistence lengths of bare DNA due to electrostatic interactions [34]. In the present case, methylation is not directly related to these electrostatic interactions. However, agreement between the data and the two-exponential model could be explained by ion adsorption onto the DNA resulting from the methylation [41]. Indeed, adsorption of hydroxide ions HO^- can lead to an increase in electrostatic persistence length due to the increase in negative charges. Alternatively, as previously suggested, local steric hindrance due to methyl groups may also explain the stiffening [42]. However, the hypothesis of local steric hindrance as the source of the observed bi-exponential behavior of the average cosine plot can be considered less probable than the assumption of ions adsorption, in view of the long-range character of the deviation. Indeed, adding the second exponential becomes indispensable to get satisfactory fits of the mean cosine distribution when the correlation step exceeds several tens of nanometers, where steric effects should be averaged out (for low fractions of methylated base-pairs). Indeed, as demonstrated by MD simulations, negative ions (in the present case Cl_2) actually adsorb onto methylated surface groups [43]. In that paper the authors observed numerically that I^- adsorbed preferentially to CH_3 decorated on surfaces and analogously Cl^- could be adsorbed on methylated Cytosine even if the effect should

be weaker. At least heuristically, these findings confirm the appropriateness of the two-exponential theoretical model for describing the data herein and suggest that the presence of methylated bases can induce modification of the charge distribution along the chain or the local bending modulus of the chain.

4. Conclusions

Cytosine methylation is a very important biochemical phenomenon that continues to warrant study and detailed analysis. A major consequence of DNA methylation is gene silencing. This epigenetic regulation mechanism relies on inhibition of the binding of transcription factors to methylated gene promoters, enhancers, or transcription start sites. The present work studied the effects of methylation on DNA morphology by analyzing quantitative AFM images. We found a noticeable increase in DNA persistence length and, therefore, rigidity upon methylation. Because the binding of transcription factors often requires local modifications in the morphology of the recognized traits, including bending, the observed morphological modification may help hamper this biochemical process, which underlies DNA transcription.

Acknowledgements

We thank D. Barisani and A. Cinti for useful advice regarding the realization of the DNA constructs. This research was supported in part by Fondo di Ateneo per la Ricerca of the University of Milano-Bicocca.

References

[1] R. Jaenisch, A. Bird, Epigenetic regulation of gene expression: how the genome integrates intrinsic and environmental signals, Nat. Genet. 33 (2003) Suppl:245–254.

[2] E. Li, C. Beard, R. Jaenisch, Role for DNA methylation in genomic imprinting, Nature 366 (1993) 362–365.

[3] Z. Smith, A. Meissner, DNA methylation: roles in mammalian development, Nat. Rev. Genet. 14 (2013) 204–220.

[4] B. Illi, R. Ciarapica, M. Capogrossi, Chromatin methylation and cardiovascular aging, J. Mol. Cell Cardiol. 83 (2015) 21–31.

[5] C. Plass, S. Pfister, A. Lindroth, O. Bogatyrova, R. Claus, P. Lichter, Mutations in regulators of the epigenome and their connections to global chromatin patterns in cancer, Nat. Rev. Genet. 14 (2013) 765–780.

[6] M. Ko, Y. Huang, A. Jankowska, U. Pape, M. Tahiliani, H. Bandukwala, J. An, E. Lamperti, K. Koh, R. Ganetzky, X. Liu, L. Aravind, S. Agarwal, J. Maciejewski, A. Rao, Impaired hydroxylation of 5-methylcytosine in myeloid cancers with mutant TET2, Nature 468 (2010) 839–843.

[7] B. Hendrich, A. Bird, Identification and characterization of a family of mammalian methyl-CpG binding proteins, Mol. Cell. Biol. 18 (1998) 6538–6547.

[8] Y. Liu, X. Zhang, R. Blumenthal, X. Cheng, A common mode of recognition for methylated CpG, Trends Biochem. Sci. 38 (2013) 177–183.

[9] T. Baubec, R. Ivanek, F. Lienert, D. Schubeler, Methylation-dependent and -independent genomic targeting principles of the MBD protein family, Cell 153 (2013) 480–492.

[10] I. Candiloro, T. Mikeska, P. Hokland, A. Dobrovic, Rapid analysis of heterogeneously methylated DNA using digital methylation-sensitive high resolution melting: application to the CDKN2B (p15) gene, Epigenetics Chromatin 1 (2008) 7.

[11] L. Kristensen, T. Mikeska, M. Krypuy, A. Dobrovic, Sensitive melting analysis after real time- methylation specific PCR (SMART-MSP): high-throughput and probe-free quantitative DNA methylation detection, Nucleic Acids Res. 36 (2008) e42.

[12] E. Smith, M. Jones, P. Drew, Quantitation of DNA methylation by melt curve analysis, BMC Cancer 9 (2009) 123.

[13] Z. Scholl, Q. Li, P. Marszalek, Single molecule mechanical manipulation for studying biological properties of proteins, DNA, and sugars, Wiley Interdiscip. Rev.: Nanomed. Nanobiotechnol. 6 (2014) 211–229.

[14] V. Cassina, D. Seruggia, G. L. Beretta, D. Salerno, D. Brogioli, S. Manzini, F. Zunino, F. Mantegazza, Atomic force microscopy study of DNA conformation in the presence of drugs, Eur. Biophys. J. 40 (2011) 59–68.

[15] M. Gregori, V. Cassina, D. Brogioli, D. Salerno, L. D. Kimpe, W. Scheper, M. Masserini, F. Mantegazza, Stability of Abeta (1-42) peptide fibrils as consequence of environmental modifications, Eur. Biophys. J. 39 (2010) 1613–1623.

[16] I. Popa, J. Fernandez, S. Garcia-Manyes, Direct quantification of the attempt frequency determining the mechanical unfolding of Ubiquitin protein, J. Biol. Chem. 286 (2011) 31072–31079.

[17] I. Popa, P. Kosuri, J. Alegre-Cebollada, S. Garcia-Manyes, J. Fernandez, Force dependency of biochemical reactions measured by single-molecule force-clamp spectroscopy, Nat. Protoc. 8 (2013) 1261–1276.

[18] M. Wanunu, D. Cohen-Karni, R. Johnson, L. Fields, J. Benner, N. Peterman, Y. Zheng, M. Klein, M. Drndic, Discrimination of methylcytosine from hydroxymethylcytosine in DNA molecules, J. Am. Chem. Soc. 133 (2011) 486–492.

[19] M. Karymov, M. Tomschik, S. Leuba, P. Caiafa, J. Zlatanova, DNA methylation-dependent chromatin fiber compaction in vivo and in vitro: requirement for linker histone, Faseb J. 15 (2001) 2631–2641.

[20] A. Mendonca, E. Chang, W. Liu, C. Yuan, Hydroxymethylation of DNA influences nucleosomal conformation and stability in vitro, BBA 1839 (2014) 1323–1329.

[21] P. Kaur, B. Plochberger, P. Costa, S. Cope, S. Vaiana, S. Lindsay, Hydrophobicity of methylated DNA as a possible mechanism for gene silencing, Phys. Biol. 9 (2012) 065001.

[22] R. Zhu, S. Howorka, J. Proll, F. Kienberger, J. Preiner, J. Hesse, A. Ebner, V. Pastushenko, H. Gruber, P. Hinterdorfer, Nanomechanical recognition measurements of individual dna molecules reveal epigenetic methylation patterns, Nat. Nanotechnol. 5 (2010) 788–791.

[23] P. Severin, X. Zou, H. Gaub, K. Schulten, Cytosine methylation alters DNA mechanical properties, Nucleic Acids Res. 39 (2011) 8740–8751.

[24] M. Endo, Y. Katsuda, K. Hidaka, H. Sugiyama, Regulation of DNA methylation using different tensions of double strands constructed in a defined DNA nanostructure, J. Am. Chem. Soc. 132 (2010) 1592–1597.

[25] J. A. Abels, F. Moreno-Herrero, T. van der Heijden, C. Dekker, N. H. Dekker, Single-molecule measurements of the persistence length of double-stranded RNA, Biophys. J. 88 (2005) 2737–2744.

[26] L. H. Pope, M. C. Davies, C. A. Laughton, C. J. Roberts, S. J. B. Tendler, P. M. Williams, Atomic force microscopy studies of intercalation-induced changes in plasmid DNA tertiary structure, J. Microsc. 199 (2000) 68–78.

[27] J. E. Coury, L. McFaillsom, L. D. Williams, L. A. Bottomley, A novel assay for drug-DNA binding mode, affinity, and exclusion number: scanning force microscopy, Proc. Natl. Acad. Sci. U.S.A. 93 (1996) 12283–12286.

[28] F. Moreno-Herrero, R. Seidel, S. M. Johnson, A. Fire, N. H. Dekker, Structural analysis of hyperperiodic DNA from Caenorhabditis elegans, Nucleic Acids Res. 34 (2006) 3057–3066.

[29] S. B. Smith, L. Finzi, C. Bustamante, Direct mechanical measurements of the elasticity of single DNA molecules by using magnetic beads, Science 258 (1992) 1122–1126.

[30] O. Kratky, G. Porod, Rontgenuntersuchung geloster fadenmolekule, Recl. Trav. Chim. Pays Bas 68 (1949) 1106–1122.

[31] P. A. Wiggins, T. van der Heijden, F. Moreno-Herrero, A. Spakowitz, R. Phillips, J. Widom, C. Dekker, P. C. Nelson, High flexibility of DNA on short length scales probed by atomic force microscopy, Nat. Nanotechnol. 1 (2006) 137–141.

[32] C. Rivetti, M. Guthold, C. Bustamante, Scanning force microscopy of DNA deposited onto mica: equilibration versus kinetic trapping studied by satistical polymer chain analysis, J. Mol. Biol. 264 (1996) 919–932.

[33] I. Jimenez-Useche, D. Shim, J. Yu, C. Yuan, Unmethylated and methylated cpg dinucleotides distinctively regulate the physical properties of DNA, Biopolymers 101 (2014) 517–524.

[34] M. Manghi, R. Netz, Variational theory for a single polyelectrolyte chain revisited, Eur. Phys. J. E Soft Matter 14 (2004) 67–77.

[35] A. Gubarev, J. Carrillo, A. Dobrynin, Scale-dependent electrostatic stiffening in biopolymers, Macromolecules 42 (2009) 5851–5860.

[36] P. Bacova, P. Kosovan, F. Uhlik, J. Kuldova, Z. Limpouchova, K. Prochazka, Double-exponential decay of orientational correlations in semiflexible polyelectrolytes, Eur. Phys. J. E 35 (2012) 53.

[37] A. Brunet, C. Tardin, L. Salome, P. Rousseau, N. Destainville, M. Manghi, Dependence of DNA persistence length on ionic strength of solutions with monovalent and divalent salts: A joint theory-experiment study, Macromolecules 48 (2015) 3641–3652.

[38] M. Banyay, A. Graslund, Structural effects of cytosine methylation on DNA sugar pucker studied by FTIR, J. Mol. Biol. 324 (2002) 667–676.

[39] A. Perez, C. L. Castellazzi, F. Battistini, K. Collinet, O. Flores, O. Deniz, M. L. Ruiz, D. Torrents, R. Eritja, M. Soler-Lopez, M. Orozco, Impact of methylation on the physical properties of DNA, Biophys. J. 102 (2012) 2140–2148.

[40] L. Nardo, M. Lamperti, D. Salerno, V. Cassina, N. Missana, M. Bondani, A. Tempestini, F. Mantegazza, Effects of non-CpG site methylation on DNA thermal stability: a fluorescence study, Nucl. Acids Res. (2015) doi: 10.1093/nar/gkv884.

[41] R. Schweiss, P. Welzel, C. Werner, W. Knoll, Dissociation of surface functional groups and preferential adsorption of ions on self-assembled monolayers assessed by streaming potential and streaming current measurements, Langmuir 17 (2001) 4304–4311.

[42] N. Toan, C. Micheletti, Inferring the effective thickness of polyelectrolytes from stretching measurements at various ionic strengths: applications to DNA and RNA, J. Phys.: Condens. Matter 18 (2006) S269.

[43] N. Schwierz, D. Horinek, R. R. Netz, Reversed anionic hofmeister series: The interplay of surface charge and surface polarity, Langmuir 26 (2010) 7370–7379.